Supporting Information

Enhancing Photovoltage of Silicon Photoanodes by a High Work-function Coordination Polymer

Ponart Aroonratsameruang,[†] Kanokwan Klahan,[†] Gabriel Loget,[‡]
Pichaya Pattanasattayavong*[,†,§]

[†]Department of Materials Science and Engineering, School of Molecular Science and Engineering, Vidyasirimedhi Institute of Science and Technology (VISTEC), Rayong, 21210, Thailand.

[‡]Univ Rennes, CNRS, ISCR (Institut des Sciences Chimiques de Rennes)-UMR6226, F-35000 Rennes, France.

[§]Research Network of NANOTEC-VISTEC on Nanotechnology for Energy, Vidyasirimedhi Institute of Science and Technology (VISTEC), Rayong, 21210, Thailand

*E-mail: pichaya.p@vistec.ac.th

Note S1: Verifying the formation of CuSCN layer

The elemental compositions of the optimal sample conditions, n-Si/SiO_x/Cu-200s and n-Si/SiO_x/Cu/CuSCN-5s, were analyzed by X-ray photoelectron spectroscopy (XPS). The XPS survey spectra confirmed the presence of all expected elements: Si, Cu, and O for n-Si/SiO_x/Cu-200s with additional N and S for n-Si/SiO_x/Cu/CuSCN-5s (Figure S2a). From the high-resolution XPS spectra, the Cu $2p_{3/2}$ and Cu $2p_{1/2}$ peaks for both electrodes were located at 932.5 and 952.4 eV (Figure S2b), respectively, agreeing with reported values.[1,2] The absence of a strong satellite suggests that Cu are either in the Cu(0) or Cu(I) states. For the thiocyanate-treated surface, the signals of S 2p and N 1s were clearly found at 163.4 and 398.6 eV, respectively (Figure S2c and d), indicating the formation of CuSCN. The O 1s peak (Figure S2e) can be attributed to SiO_x and the thin native copper oxide (CuO_x) that spontaneously forms over the Cu surface under ambient conditions.[3]

We note that the S 2p peak shows a complex structure compared to the general feature of S $2p_{1/2}$ and S $2p_{3/2}$ doublet.[2,4] This can be attributed to the possible formation of native defects, such as M-NCS.[5] Indeed, the two types of M-SCN and M-NCS bonding would result in different S 2p binding energies.[6] The S 2p region was thus deconvoluted into two pairs of doublets having a $2p_{1/2}$ – $2p_{3/2}$ doublet separation value of 1.2 eV (Figure S2f). Indeed, the two deconvoluted S $2p_{3/2}$ peaks at 163.5 and 162.0 eV are comparable to the literature values of the sulfur binding energies in M-SCN and M-NCS, respectively.[4,7]

The presence of the CN group was also confirmed by Raman spectroscopy. In Figure S3a, the Raman signal of FTO/Cu/CuSCN was detected at 2175 cm^{-1}, consistent with the stretching vibrations of the C≡N bond in Cu-SCN.[8] Furthermore, the ultraviolet-visible (UV-Vis) reflectance spectra (Figure S3b) showed that n-Si/SiO_x/Cu/CuSCN-5s exhibited notably reduced reflectance in the UV region (30-45% below 400 nm), compared to those of n-Si and n-Si/SiO_x/Cu-200s (>60%). The reflectivity loss can be attributed to the absorption of CuSCN, which occurs in the UV due to its large band gap.[4] The data from XPS, Raman spectroscopy, and UV-Vis spectroscopy collectively confirm the formation of CuSCN.

Note S2: Stability of Cu-modified Si photoanodes

To investigate the stability of our photoanodes during the oxygen evolution reaction (OER), chronopotentiometry was performed under simulated sunlight at a current density of 2 mA cm^{-2}. The n-Si/SiO_x/Cu/CuSCN photoanode initially required a smaller applied potential than n-Si/SiO_x/Cu (Figure S11a). However, at longer times, the potentials of both photoanodes increased rapidly (Figure S11b) approximately after 100 and 200 s for n-Si/SiO_x/Cu/CuSCN and n-Si/SiO_x/Cu, respectively. The issue with stability during OER was also observed in cyclic voltammetry (CV) measurements; after nine cycles, the photocurrents of both n-Si/SiO_x/Cu and n-Si/SiO_x/Cu/CuSCN dropped to ~70% of their initial current values (Figure S12).

The n-Si/SiO_x/Cu/CuSCN photoanode after nine CV cycles (designation: 9cy) under simulated sunlight was also studied with XPS and compared with the results of the sample before the CV measurements (designation: 0cy) as shown in Figure S13. The XPS wide scans (Figure S13a) show significant changes in the chemical states and composition after the OER runs. The relative intensities of Cu peaks decreased which is possibly due to the loss of Cu (also corroborated by the experiment on FTO/Cu discussed in the next paragraph). We also note that Si signals appeared drastically more prominent, substantiating that the substrate became more exposed. The oscillations following Si 2s and Si 2p peaks can be assigned to plasmon losses.[9] For the remaining Cu, the oxidation of Cu(I) to Cu(II) can be clearly seen as the satellite feature appeared (Figure S13b). Considering the Cu $2p_{3/2}$ state in more detail, the data of the 0cy sample was identified as a single peak of Cu(I) at a binding energy of 932.5 eV (Figure S13c). After the OER, the 9cy sample could be fitted with two states at 932.5 eV and 933.9 eV (Figure S13d), assigned to Cu(I) and Cu(II), respectively.[10] The chemical states of the thiocyanate ligand could no longer be found. Both the S 2p and N 1s peaks disappeared following nine cycles of PEC runs (Figure S13e-f). The O 1s signal also changed although specific assignments were complicated by the possibility of various O-containing species. The remaining Cu species likely existed as CuO_x.

We also checked the stability of a non-photoactive FTO/Cu electrode by running CV in the dark. After 20 cycles, the current gradually decreased to ~85% of the initial photocurrent (Figure S14a). SEM images before and after 20-cycle CV show that the particle amount and size of the OER-tested FTO/Cu apparently decreased when compared to those of the fresh FTO/Cu (Figure S14b and c). This evidence strongly indicates that the instability of our photoelectrodes is likely resulted from Cu corrosion.[11]

Note S3: XPS characterization of as-sputtered and photoelectrochemically dissolved Cu

The as-sputtered n-Si/SiO_x/Cu samples before and after the PEC dissolution were also investigated by XPS (Figure S17a). For the modified electrode, the O 1s region (Figure S17b) featured an additional component at 529.7 eV, which could be assigned CuO_x.[12] In the Cu 2p binding energy region (Figure S17c), the presence of the satellite in the PEC-dissolved sample also indicated the presence of Cu(II) due to CuO_x. Performing peak fitting of the Cu $2p_{3/2}$, the as-sputtered sample yielded two peaks at 932.7 eV and 933.5 eV, belonging to Cu and CuO_x (Figure S17d),[1,12] respectively. The modified electrode also featured two states (Figure S17e), but the CuO_x peak became significantly more prominent compared to the as-sputtered sample.

References

(1) Shi, Y.; Gimbert-Suriñach, C.; Han, T.; Berardi, S.; Lanza, M.; Llobet, A. CuO-Functionalized Silicon Photoanodes for Photoelectrochemical Water Splitting Devices. *ACS Appl. Mater. Interfaces* **2016**, *8* (1), 696–702. https://doi.org/10.1021/acsami.5b09816.

(2) Worakajit, P.; Hamada, F.; Sahu, D.; Kidkhunthod, P.; Sudyoadsuk, T.; Promarak, V.; Harding, D. J.; Packwood, D. M.; Saeki, A.; Pattanasattayavong, P. Elucidating the Coordination of Diethyl Sulfide Molecules in Copper(I) Thiocyanate (CuSCN) Thin Films and Improving Hole Transport by Antisolvent Treatment. *Adv. Funct. Mater.* **2020**, *30* (36), 2002355. https://doi.org/10.1002/adfm.202002355.

(3) Wang, J.-G.; Shi, L.; Su, Y.; Liu, L.; Yang, Z.; Huang, R.; Xie, J.; Tian, Y.; Li, D. In-Situ Plasmonic Tracking Oxygen Evolution Reveals Multistage Oxygen Diffusion and Accumulating Inhibition. *Nat. Commun.* **2021**, *12* (1), 2164. https://doi.org/10.1038/s41467-021-22434-3.

(4) Pan, L.; Liu, Y.; Yao, L.; Dan Ren; Sivula, K.; Grätzel, M.; Hagfeldt, A. Cu2O Photocathodes with Band-Tail States Assisted Hole Transport for Standalone Solar Water Splitting. *Nat. Commun.* **2020**, *11* (1), 318. https://doi.org/10.1038/s41467-019-13987-5.

(5) Tsetseris, L. Copper Thiocyanate: Polytypes, Defects, Impurities, and Surfaces. *J. Phys. Condens. Matter* **2016**, *28* (29), 295801. https://doi.org/10.1088/0953-8984/28/29/295801.

(6) Walton, R. A. X-Ray Photoelectron Spectra of Inorganic Molecules [1]. XXIII. On the Question of the Usefulness of XPS in Studying the Ambidentate Nature of the Thiocyanate Ligand. *Inorganica Chim. Acta* **1979**, *37* (C), 237–240. https://doi.org/10.1016/S0020-1693(00)95550-6.

(7) Wechwithayakhlung, C.; Packwood, D. M.; Chaopaknam, J.; Worakajit, P.; Ittisanronnachai, S.; Chanlek, N.; Promarak, V.; Kongpatpanich, K.; Harding, D. J.; Pattanasattayavong, P. Tin(<scp>ii</Scp>) Thiocyanate $Sn(NCS)_2$ – a Wide Band Gap Coordination Polymer Semiconductor with a 2D Structure. *J. Mater. Chem. C* **2019**, *7* (12), 3452–3462. https://doi.org/10.1039/C8TC06150E.

(8) Aldakov, D.; Chappaz-Gillot, C.; Salazar, R.; Delaye, V.; Welsby, K. A.; Ivanova, V.; Dunstan, P. R. Properties of Electrodeposited CuSCN 2D Layers and Nanowires Influenced by Their Mixed Domain Structure. *J. Phys. Chem. C* **2014**, *118* (29), 16095–16103. https://doi.org/10.1021/jp412499f.

(9) Haasch, R. T. X-Ray Photoelectron Spectroscopy (XPS) and Auger Electron Spectroscopy (AES). In *Practical Materials Characterization*; Sardela, M., Ed.; Springer New York: New York, NY, 2014; pp 93–132. https://doi.org/10.1007/978-1-4614-9281-8_3.

(10) NIST X-ray Photoelectron Spectroscopy Database, NIST Standard Reference Database Number 20, National Institute of Standards and Technology, Gaithersburg MD, 20899 (2000). https://doi.org/10.18434/T4T88K.

(11) Gawande, M. B.; Goswami, A.; Felpin, F.-X.; Asefa, T.; Huang, X.; Silva, R.; Zou, X.; Zboril, R.; Varma, R. S. Cu and Cu-Based Nanoparticles: Synthesis and Applications in Catalysis. *Chem. Rev.* **2016**, *116* (6), 3722–3811. https://doi.org/10.1021/acs.chemrev.5b00482.

(12) Deroubaix, G.; Marcus, P. X-Ray Photoelectron Spectroscopy Analysis of Copper and Zinc Oxides and Sulphides. *Surf. Interface Anal.* **1992**, *18* (1), 39–46. https://doi.org/10.1002/sia.740180107.

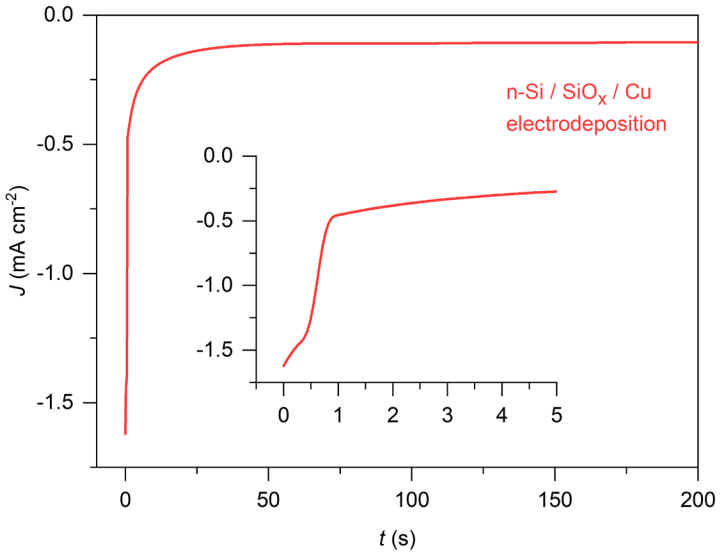

Figure S1. Chronoamperometry curve of Cu electrodeposition on freshly etched n-Si. The inset shows the data in the first 5 seconds.

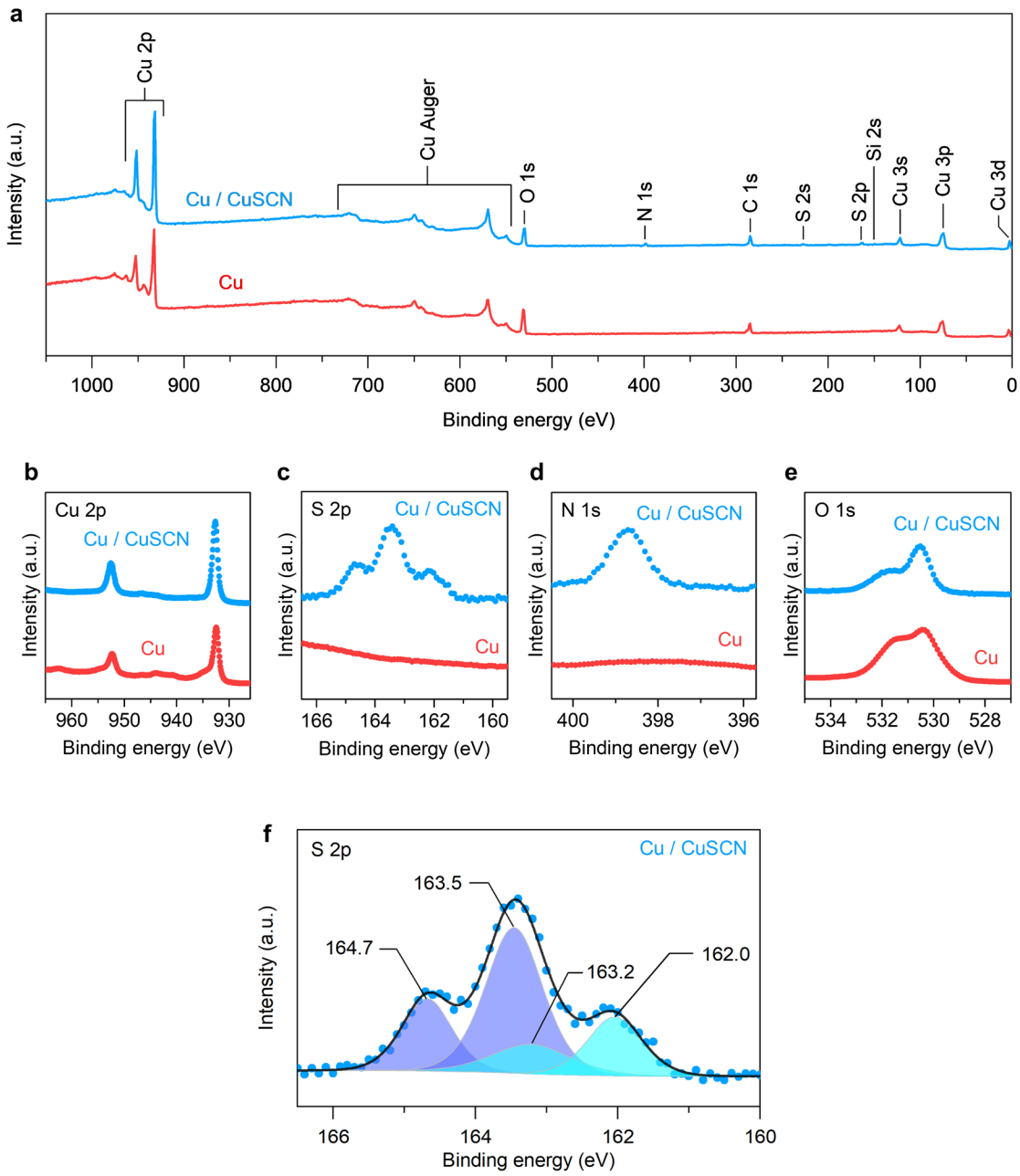

Figure S2. (a) XPS survey and core-level scans of (b) Cu 2p, (c) S 2p, (d) N 1s, (e) and O 1s recorded for n-Si/SiO_x/Cu-200s (red) and n-Si/SiO_x/Cu/CuSCN-5s (blue). (f) Deconvoluted S 2p core-level spectrum of n-Si/SiO_x/Cu/CuSCN-5s. The scattered points are the collected data, the shaded areas the fitted peaks, and the solid lines the reconstructed spectrum.

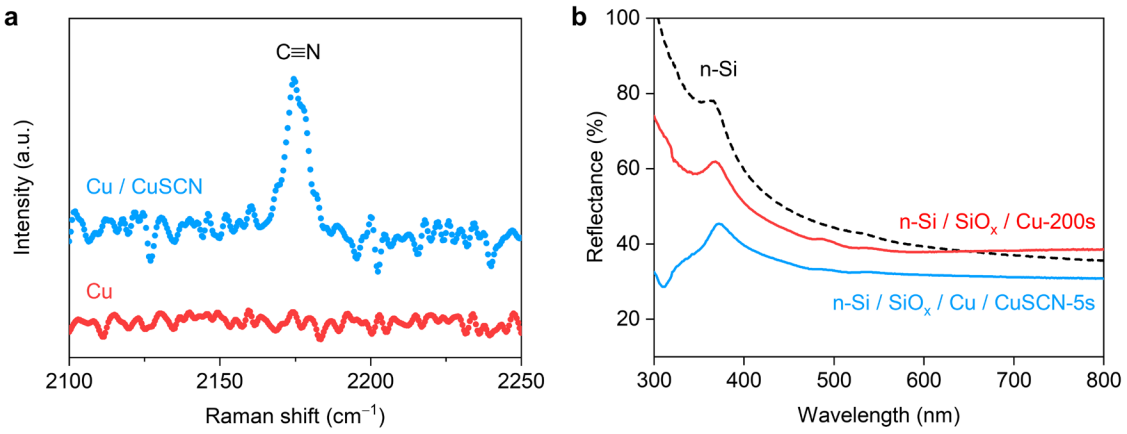

Figure S3. (a) Raman spectra of FTO/Cu (red) and FTO/Cu/CuSCN (blue). (b) UV-Vis-NIR diffuse reflectance spectra of n-Si (black dashed line), n-Si/SiO_x/Cu-200s (red solid line), and n-Si/SiO_x/Cu/CuSCN-5s (blue solid line).

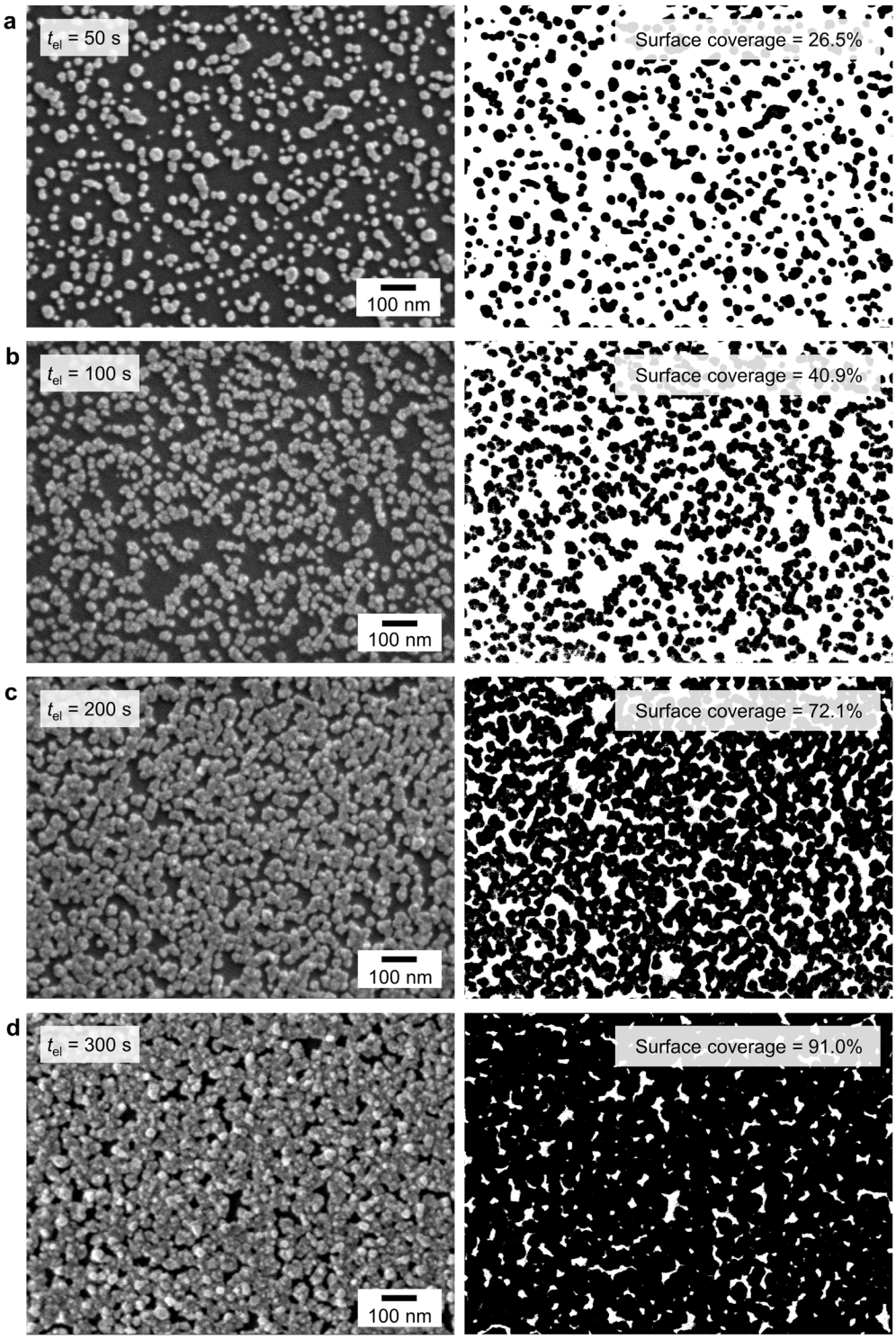

Figure S4. SEM images of n-Si with different Cu electrodeposition times (t_{el}) of (a) 50 s, (b) 100 s, (c) 200 s and (d) 300 s. All images were converted into binary data for calculating the surface coverage using ImageJ software. The mean diameter of Cu NPs was slightly changed from 24±6 nm for t_{el} = 50 s to 30±5 nm for t_{el} = 200 s. At t_{el} = 300 s, the NPs coalesced. Accordingly, the geometrical surface coverage dramatically increased from 27% for t_{el} = 50 s to 91% for t_{el} = 300 s.

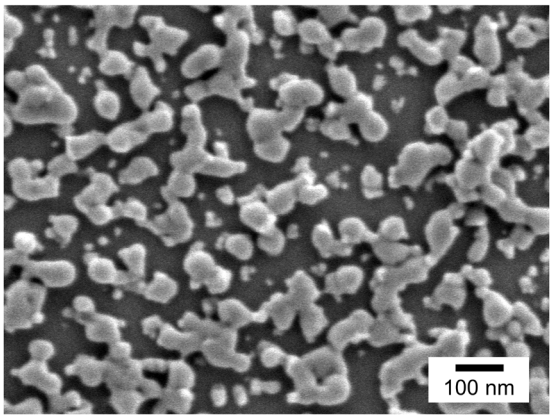

Figure S5. SEM image of n-Si/SiO_x/Cu/CuSCN-60s.

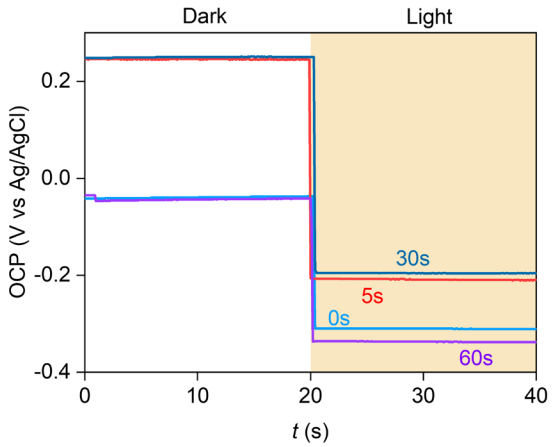

Figure S6. Dark/light open-circuit potential (OCP) measurements of n-Si/SiO_x/Cu/CuSCN-t_{ch} in a solution containing of 5/5 mM ferri/ferrocyanide and 1 M KCl.

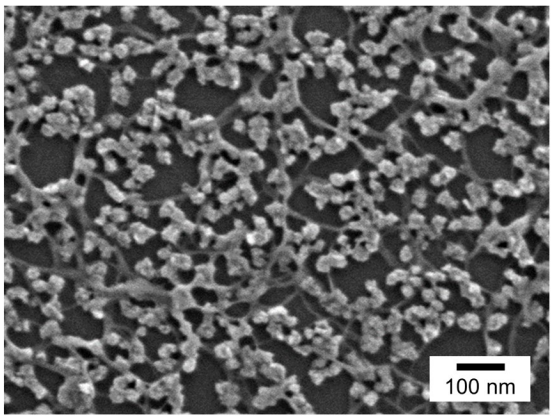

Figure S7. SEM image of n-Si/SiO_x/Cu/CuSCN-5s after soaking in diethyl sulfide (DES).

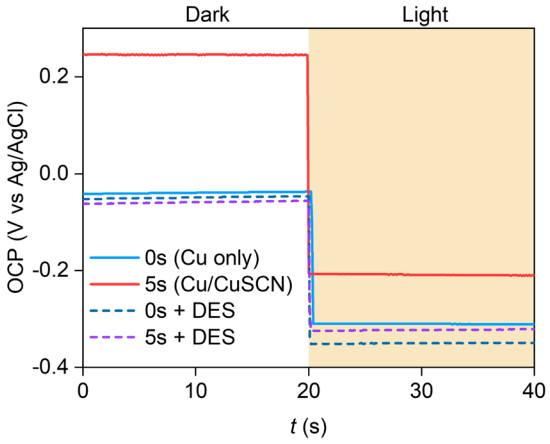

Figure S8. Dark/light open-circuit potential (OCP) measurements of n-Si/SiO_x/Cu/CuSCN-0s (Cu only) and 5s (Cu/CuSCN) before (solid lines) and after (dashed lines) soaking in DES for 5 min. The electrolyte solution contained of 5/5 mM ferri/ferrocyanide and 1 M KCl.

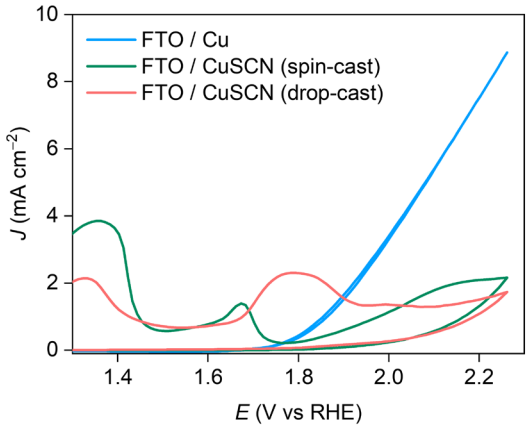

Figure S9. Cyclic voltammograms at 100 mV s^{-1} of FTO/Cu, FTO/CuSCN (spin-cast), and FTO/CuSCN (drop-cast) recorded in Li-borate/K-borate buffer in the dark. The comparison of phase-pure Cu and CuSCN on non-photoactive FTO allowed the identification of the active species for OER electrocatalysis. Cu was deposited on an FTO substrate by the same electrodeposition method. CuSCN was spin-coated or drop-cast using our previous protocols reported elsewhere.[2] Only the FTO/Cu electrode showed OER activity under applied bias, indicating that Cu is the active OER electrocatalyst in our electrode system.

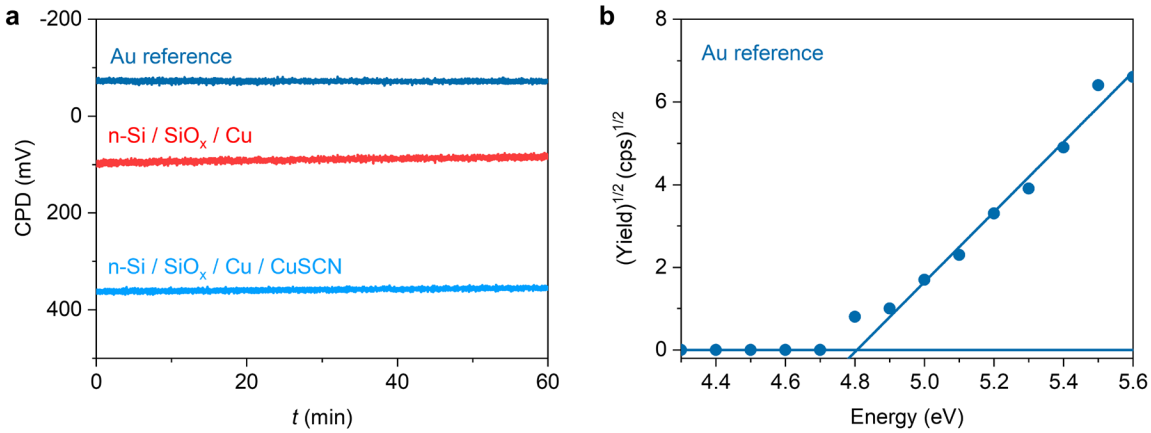

Figure S10. (a) Contact potential difference (CPD) recorded by Kelvin Probe measurements of an Au reference, n-Si/SiO_x/Cu, and n-Si/SiO_x/CuSCN. (b) Photoelectron yield spectrum of the Au reference for the determination of Au work function. The surface work functions of n-Si/SiO_x/Cu and n-Si/SiO_x/CuSCN can then be calculated from the differential CPD values with respect to the Au reference and found to be 4.96 and 5.23 eV, respectively. The measurements were performed in ambient conditions.

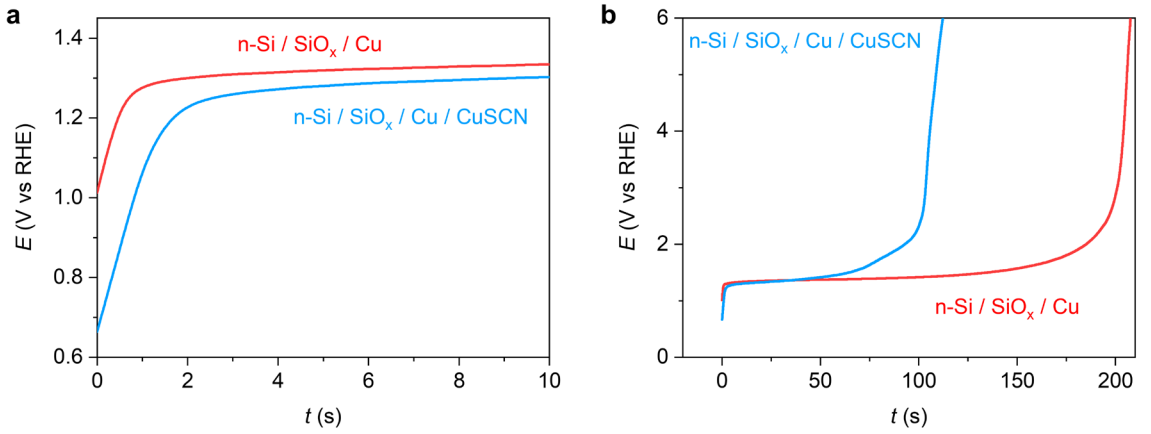

Figure S11. Chronopotentiograms shown for (a) short and (b) long time windows during the electrolysis of (red) n-Si/SiO_x/Cu and (blue) n-Si/SiO_x/Cu/CuSCN in Li-borate/K-borate buffer at a current density of 2 mA cm^{-2} under simulated sunlight.

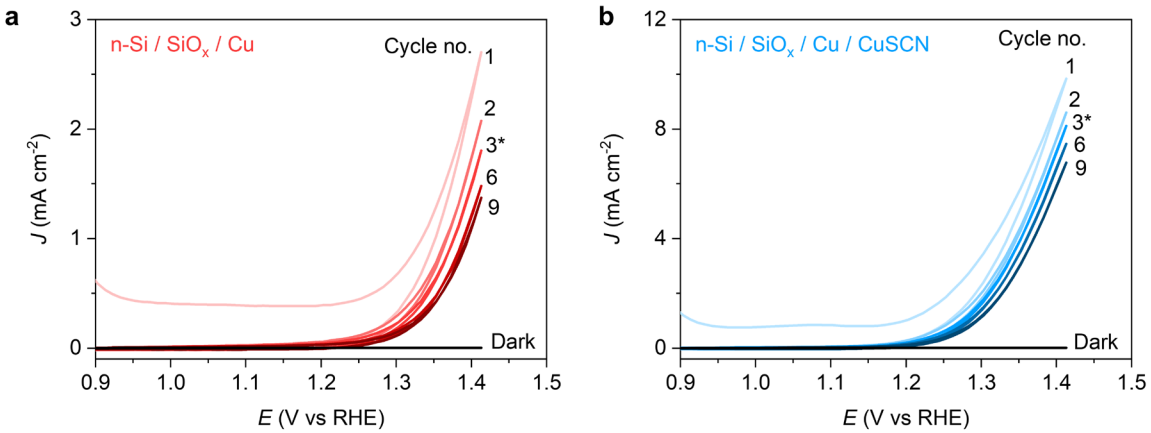

Figure S12. Cyclic voltammograms recorded at 100 mV s^{-1} under simulated sunlight of (a) n-Si/SiO_x/Cu and (b) n-Si/SiO_x/Cu/CuSCN in Li-borate/K-borate buffer. We note that the data from the 3rd cycle (marked with *) was chosen to report in the main text.

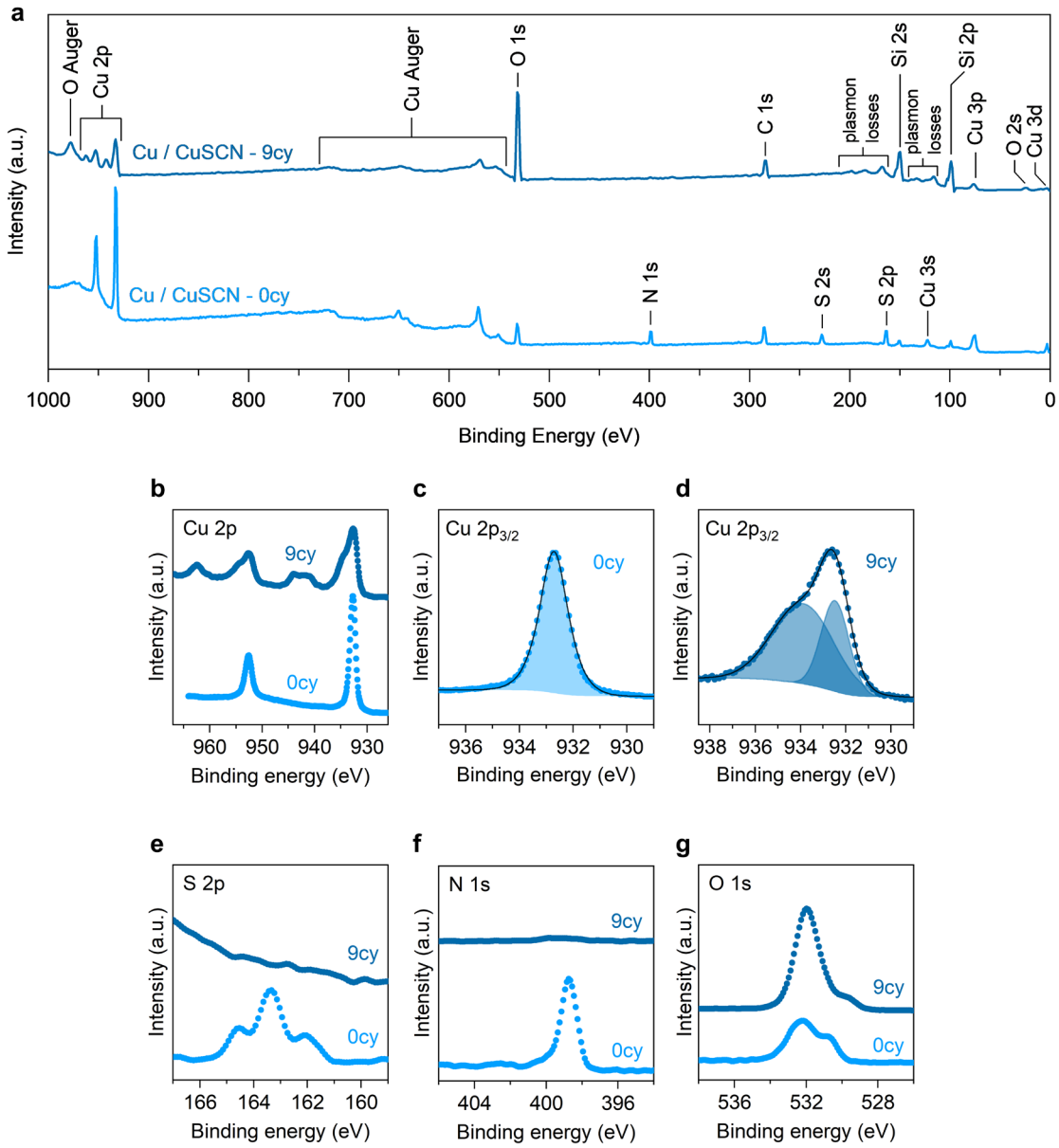

Figure S13. (a) XPS survey and core-level scans of (b)-(d) Cu 2p, (e) S 2p, (f) N 1s, (g) and O 1s recorded for n-Si/SiO_x/Cu/CuSCN before (0cy) and after nine cycles (9cy) of cyclic voltammetry under simulated sunlight. The fitting of the Cu $2p_{3/2}$ state is shown in (c) and (d). The scattered points are the collected data, the shaded areas the fitted peaks, and the solid lines the reconstructed spectrum.

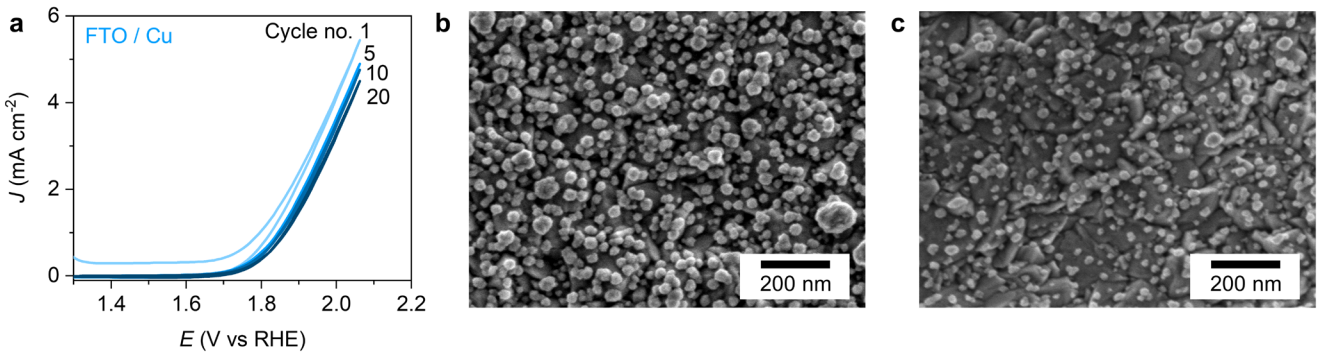

Figure S14. (a) Cyclic voltammograms recorded at 100 mV s^{-1} of FTO/Cu. SEM images of FTO/Cu (b) before and (c) after 20 cycles.

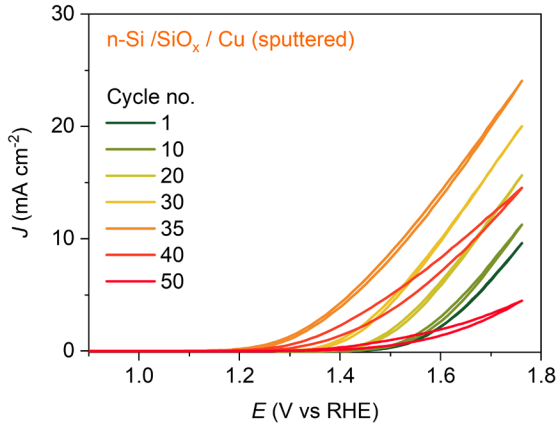

Figure S15. Cyclic voltammograms recorded at 100 mV s^{-1} under simulated sunlight of the sputtered n-Si/SiO_x/Cu in Li-borate/K-borate buffer.

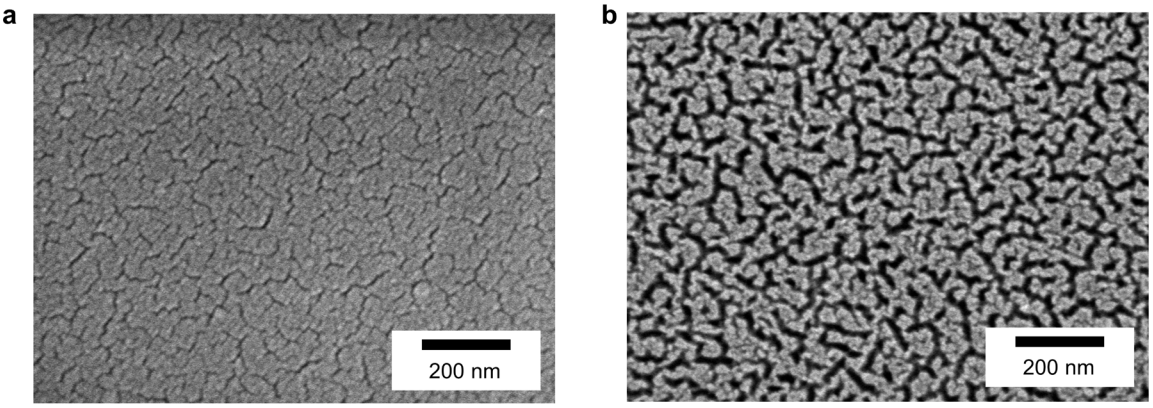

Figure S16. SEM images of the sputtered n-Si/SiO_x/Cu electrodes (a) before and (b) after modification by the PEC dissolution method.

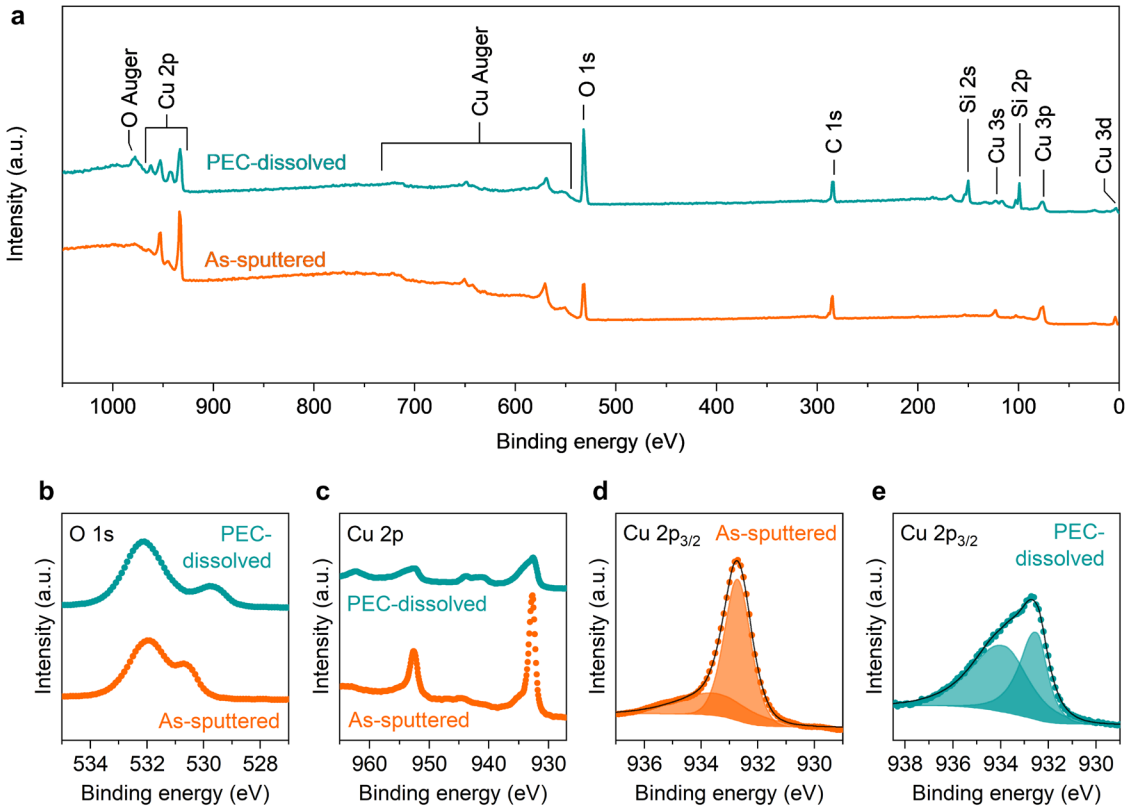

Figure S17. (a) XPS survey and core-level scans of (b) O 1s and (c) Cu 2p states of the sputtered n-Si/SiO_x/Cu electrodes before and after modification by the PEC dissolution method. Deconvoluted Cu $2p_{3/2}$ peak (d) before and (e) after the PEC dissolution. The scattered points are the collected data, the shaded areas the fitted peaks, and the solid lines the reconstructed spectra.